X-Ray Evidence for the Interaction of the Giant Elliptical Galaxy NGC 4472 with its Virgo Cluster Environment

Jimmy A. Irwin – University of Virginia
Craig L. Sarazin – University of Virginia

Citation of published version:

Irwin, J., Sarazin, C. (1996): X-Ray Evidence for the Interaction of the Giant Elliptical Galaxy NGC 4472 with its Virgo Cluster Environment. *The Astrophysical Journal*, 471(2). DOI: 10.1086/177998

THE ASTROPHYSICAL JOURNAL, 471:683–693, 1996 November 10

X-RAY EVIDENCE FOR THE INTERACTION OF THE GIANT ELLIPTICAL GALAXY NGC 4472 WITH ITS VIRGO CLUSTER ENVIRONMENT

JIMMY A. IRWIN AND CRAIG L. SARAZIN
Department of Astronomy, University of Virginia, P.O. Box 3818, Charlottesville, VA 22903-0818; jai7e@virginia.edu, cls7i@virginia.edu
Received 1996 March 26; accepted 1996 June 10

ABSTRACT

We analyze X-ray spatial and spectral data on the giant elliptical galaxy NGC 4472, the brightest galaxy in the Virgo cluster. The X-ray contours of NGC 4472 are elongated in the northeast-southwest direction, perhaps as a result of motion through the Virgo intracluster gas. A bow shock–like structure is evident on the galaxy's north side. The temperature at a given radius in this bow shock region is slightly higher than the temperature at the same radius on the galaxy's southwest side. Away from this bow shock region, the surface brightness profile of NGC 4472 can be traced out to a radius of 260 kpc in the southwest direction. Beyond 260 kpc, we find evidence for emission from both the Virgo cluster and the Galactic North Polar Spur (believed to be the rim of a hot Galactic superbubble).

NGC 4472 is interacting with the dwarf irregular galaxy UGC 7636. We do not detect any excess or deficit in the X-ray emission toward this galaxy. An H I cloud, detected previously in the 21 cm line and located midway between the two galaxies, appears to have been removed from the irregular galaxy through either tidal interaction or ram pressure stripping. We find a marginally significant hole in the *ROSAT* HRI and PSPC X-ray images at the position of this cloud, suggesting that the cloud lies at the front side of NGC 4472. If the hole in the X-ray images is due to soft X-ray absorption, the total gaseous mass of the cloud must be at least $1.7 \times 10^9\ M_\odot$, far greater than its 21 cm H I mass. This suggests that the majority of the material in the cloud is molecular.

Subject headings: galaxies: clusters: individual (Virgo) — galaxies: individual (NGC 4472, UGC 7636) — galaxies: interactions — galaxies: ISM — X-rays: galaxies

1. INTRODUCTION

The discovery of large amounts of hot, X-ray–emitting gas associated with elliptical galaxies by the *Einstein* Observatory (Forman et al. 1979) dispelled the long-held notion that elliptical galaxies were devoid of any significant amount of interstellar material. X-ray emission from a ~ 1 keV thermal plasma was found to be quite common among bright early-type galaxies (see, e.g., Forman, Jones, & Tucker 1985; Trinchieri, Fabbiano, & Canizares 1986). This hot gas provides a powerful means of deducing the total gravitational mass of an elliptical galaxy to larger radii than can generally be determined optically. The improved spatial and spectral resolution of the *ROSAT* Observatory has allowed for more accurate determinations of the total mass. This has led to the conclusion that some elliptical galaxies possess a massive dark halo similar to those detected in spiral galaxies (see, e.g., Kim & Fabbiano 1995), although this idea is still somewhat controversial.

X-rays also provide an important means of studying how elliptical galaxies are interacting not only with other components of the galaxy but also with their environment. Joint X-ray and radio observations of the elliptical galaxy NGC 1399, for example, indicate that radio jets emanating from the nucleus are coincident with a "tunnel" in the hot X-ray–emitting gas (Kim et al. 1995), suggesting that the radio jets are being confined by the hot interstellar medium (ISM). Similarly, a deficit in the soft X-ray flux in this same galaxy may indicate that a large amount ($\sim 10^{12}\ M_\odot$) of cold absorbing matter is present, which is not currently detectable at any other wavelength (Rangarajan et al. 1995). Clearly, much information can be gleaned from X-ray observations about the non–X-ray–emitting material associated with elliptical galaxies.

Far from being an isolated elliptical galaxy, the X-ray emission detected in the direction of the Virgo elliptical galaxy NGC 4472 is a result of several distinct components. Besides the ~ 1 keV gas associated with the galaxy itself, there is emission from underlying Virgo intracluster gas in which NGC 4472 is embedded (Koyama, Takano, & Tawara 1991; Böhringer et al. 1994). X-ray emission from the North Polar Spur, believed to be the rim of a Galactic superbubble, is also located toward the direction of the galaxy (Böhringer et al. 1994). Finally, NGC 4472 is currently interacting with the dwarf irregular galaxy UGC 7636, from which a cloud of H I gas lying midway between the two galaxies seems to have been removed (Sancisi et al. 1987; Patterson & Thuan 1992; McNamara et al. 1994). Below we present evidence for X-ray absorption due to this gas cloud.

This paper is organized as follows. In § 2 we describe the X-ray observations made by the *ROSAT* HRI and PSPC. The global appearance of the galaxy is described in § 3. In § 4 the temperature profile is presented, as well as the spectral analysis of the background emission surrounding NGC 4472. The spatial analysis of the NGC 4472/UGC 7636 system is presented in § 5. A possible absorption feature in the X-ray image at the position of the H I cloud is discussed in § 5.4. The interpretation of the distorted X-ray structure of NGC 4472 and the cloud of H I that appears to have been stripped from UGC 7636 is discussed in § 6. Our results are summarized in § 7.

2. X-RAY OBSERVATIONS

Our observation of NGC 4472 with the *ROSAT* HRI (High-Resolution Imager) was made in the two periods of 1992 December 10–14 and 1994 June 19–July 9 for a total

exposure of 34,129 s. The two observations were combined by simultaneously matching the positions of the peak in emission and several serendipitous point sources located north and south of the peak in emission in both observational intervals. Periods of high background near the beginning and end of the observation intervals were removed, leaving 31,159 s of useful observation time. We have supplemented our HRI data with *ROSAT* PSPC (Position Sensitive Proportional Counter) data from the public archive. This observation (RP600248, Principal Investigator C. Jones) consists of an exposure of 25,971 s taken over the period 1992 December 26–29. The original analysis of these observations was published in Forman et al. (1993), which concentrated on the analysis of the heavy-element abundance and its gradient in the gas. We will use the same data to provide spectral information and more extended surface brightness information to complement our HRI observation. Before analyzing the PSPC data, periods of high background due to charged particles were removed by filtering the PSPC data such that all time intervals with a Master Veto Rate above 170 counts s^{-1} were excluded (see Plucinsky et al. 1993 for a description of the charged particle rejection efficiency of the PSPC). Periods of short-term background enhancements (due in part to auroral X-rays and solar flaring) were also removed, resulting in an effective exposure of 21,806 s. The PSPC data were divided into soft and hard bands. The soft band covers the 0.2–0.42 keV energy range, and the hard band covers the 0.52–2.02 keV energy range (bands 1–2 and 4–7, respectively, in the Snowden 1995 nomenclature). The spectral analysis in this study was performed using XSPEC, and the spatial analysis was performed in part using the PROS package within IRAF. We assume that NGC 4472 and the Virgo cluster are at a distance of 25.8 Mpc (Faber et al. 1989), which is the value appropriate for a Hubble constant of $H_0 = 50$ km s^{-1} Mpc^{-1}. At this distance, 1′ corresponds to 7.5 kpc.

3. GLOBAL APPEARANCE

In order to take advantage of the higher spatial resolution of the HRI and the greater sensitivity and wider field of view of the PSPC, we have merged the two data sets to produce an image of the entire galaxy and its surroundings. Figure 1 shows a smoothed, background-subtracted contour plot of the merged PSPC + HRI image superposed on an optical image of the galaxy from the Digital Sky Survey. This map was created by first smoothing the PSPC and HRI images separately using an adaptive kernel density estimation method (Huang & Sarazin 1996). A constant signal-to-noise ratio of 5 was used to determine the smoothing length of the Gaussian beam. After normalizing the HRI count rate to the PSPC count rate, the two images were merged in the following manner. The HRI image was

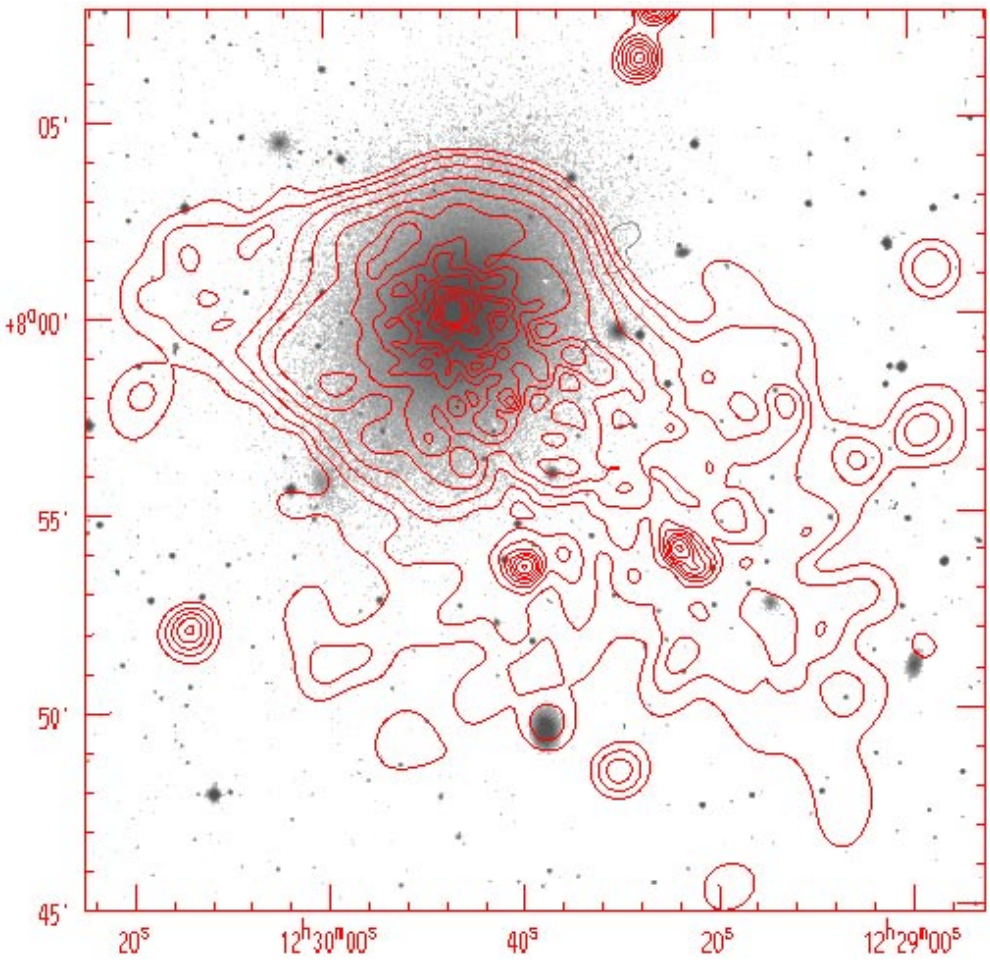

FIG. 1.—Contour plot of the merged HRI + PSPC X-ray image band after adaptive kernel smoothing superposed on an optical image of the galaxy from the Digital Sky Survey. A constant S/N of 5 per smoothing beam was used to determine the smoothing length. The coordinates are R.A. and decl. (J2000). Note the bow shock feature to the north of the peak in emission and the general asymmetry of the X-ray emission.

multiplied by the function $f(r)$ and the PSPC by the function $1-f(r)$, where $f(r)=1$ for $r<4'$ and $f(r)=\exp[-(r-4')^2/\sigma^2]$ for $r>4'$, where σ was chosen such that $f(r)=0.25$ at $r=6'$. The two resulting images were then added together to yield the final image. This method provides for a smooth transition between the HRI and PSPC images.

The asymmetric nature of the X-ray emission initially discovered with *Einstein* (Forman et al. 1985) is apparent. Although the innermost contours are circular, the emission is elongated in the northeast-southwest direction at larger radii. The elongation in the X-ray image is nearly perpendicular to the optical major axis of the galaxy (King 1978). In addition to the overall elongation, the X-ray surface brightness at the north side of the galaxy falls off very rapidly. This shows up as a strong bunching of the X-ray contours at the northern edge of the galaxy in Figure 1. In order to see whether most of the distortion in the shape of the galaxy could be a result of this compression of the contours on the north side, we reflected the emission in the southern half of the galaxy across a line running east-west through the peak of emission, replacing the emission from the northern half in the process. The resulting image was largely circularly symmetric, but there was still excess low–surface brightness emission at large radii in the southwest quadrant of the galaxy. The bunching of the contours to the north is quite strong; the surface brightness drops to 0.8% of the peak value within 4′ of the center of the galaxy at the north, while it drops to this level only out at a radius of 6.′8 to the southwest. In § 6.1 we will argue that this asymmetry in the X-ray surface brightness of NGC 4472 can most reasonably be explained as a result of motion of NGC 4472 to the north through Virgo intracluster gas.

Many foreground/background point sources (presumably mainly unrelated to NGC 4472) are visible in the field of view. These point sources have been excluded from all spatial and spectral analyses. One "source" located 3.′1 southeast of the peak of emission is actually a hole in the X-ray emission. This feature will be discussed in detail in § 5.4.

4. SPECTRAL ANALYSIS OF GALACTIC AND BACKGROUND EMISSION

4.1. *Temperature Profile of NGC 4472*

Spectral fits were performed on concentric annular slices centered on NGC 4472 out to a radius of 18′ (where the rib support structure begins) and between position angles 150° and 270° measured counterclockwise from north. The restriction to this angular slice was done to avoid the distorted X-ray emission to the north, since this emission may reflect interactions of the gas in NGC 4472 with its environment (see §§ 3 and 6). The annuli were chosen such that each was larger than the joint XRT and PSPC point-spread function (Hasinger et al. 1992) and contained enough counts to determine accurately the temperature of the annulus. The spectra of the annuli were corrected for vignetting and particle background according to the Plucinsky et al. (1993) parameterization of the average Master Veto Rate of the observation. A background spectrum, extracted from an annulus of 35′–45′ (260–340 kpc) and corrected for vignetting, was scaled to and subtracted from each source spectrum. The energy channels were rebinned to contain at least 20 counts, and all channels below 0.2 keV (pulse invariant [PI] channels <20) were ignored in the fit, since the equations governing the charged particle parameterization are not applicable in that region of the spectrum. The angular extent and number of X-ray counts of each of the six annuli are listed in Table 1.

The spectra of the annular slices were fitted with a Raymond-Smith thermal plasma model (Raymond & Smith 1977) with a photoelectric absorption component (Morrison & McCammon 1983) fixed at the Galactic neutral hydrogen column density value ($N_{\rm H}=1.64\times10^{20}$ cm^{-2}; Stark et al. 1992). The abundance, temperature, and normalization of the Raymond-Smith component were allowed to vary. Acceptable fits were found for all annular slices. The best-fitting temperature T, abundance, and minimum χ^2 values for each slice are summarized in Table 1. The uncertainties represent the 90% confidence ranges for one interesting parameter ($\Delta\chi^2_{\rm min}=2.71$). Our results are consistent with those obtained by Forman et al. (1993), who used the full azimuthal range to derive their results instead of just the undisturbed region. We confirm the result that a roughly constant abundance consistent with solar is obtained if the column density is fixed at the Galactic value. Allowing the column density to vary did not significantly improve the fits. A decrease in temperature in the inner regions was found, typical of a galaxy with a cooling flow.

We wish to use the observed temperature profile to deproject the X-ray surface brightness to obtain the gas density. Because the X-ray surface brightness can be determined within smaller annuli than the spectrum, it is useful to have a smooth functional fit to the observed temperature profile. We found that a power law with an exponent of 0.127 fit the data well. The data points and the best-fit power law are shown in Figure 2.

4.2. *North Polar Spur and Virgo Emission in the Background Annulus*

Since NGC 4472 lies in the direction of the North Polar Spur (NPS) and is embedded in Virgo intracluster gas (Böhringer et al. 1994), we searched for spectral evidence of these two components in the background annulus (35′–45′). In order to subtract off the cosmic X-ray background component, a spectrum was extracted from an annulus of 35′–45′ from another region of the sky (a pointed observation of Markarian 279) with the same Galactic column density as in the direction of NGC 4472 and subtracted from the background spectrum.

A Raymond-Smith model with the abundance set at 10% of the solar value (*Ginga* found a low abundance for the Virgo cluster at large radii from M87; Koyama et al. 1991), a column density fixed at the Galactic value, and a variable temperature and normalization was used to fit the emission due to Virgo gas. A Raymond-Smith model with the abun-

TABLE 1

SPECTRAL FITS IN ANNULI

Annulus (arcmin)	Counts	kT (keV)	Abundance ($Z/Z_\odot$)	χ^2	Degrees of Freedom
0–1	2297	$0.82^{+0.03}_{-0.03}$	$0.42^{+0.08}_{-0.06}$	76.6	77
1–2.5	2651	$1.01^{+0.03}_{-0.04}$	$1.27^{+0.38}_{-0.27}$	85.9	82
2.5–4	2318	$1.09^{+0.02}_{-0.03}$	$1.20^{+0.39}_{-0.24}$	94.6	80
4–7	2472	$1.13^{+0.05}_{-0.02}$	$1.19^{+0.42}_{-0.28}$	83.6	82
7–12	2024	$1.29^{+0.10}_{-0.14}$	$1.15^{+0.72}_{-0.40}$	85.5	69
12–18.....	1581	$1.24^{+0.14}_{-0.13}$	>0.82	49.1	53

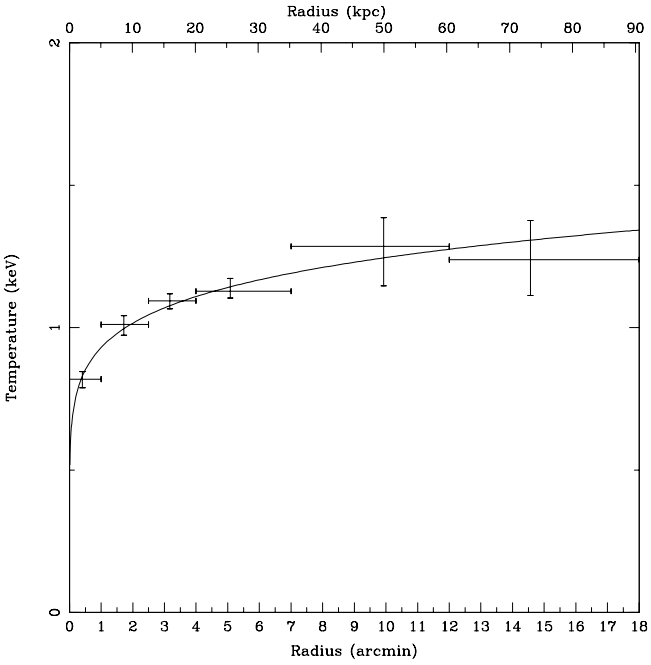

FIG. 2.—Temperature profile of NGC 4472 derived from the PSPC spectral analysis. Error bars are the 90% confidence regions for a single interesting parameter. The solid line represents the function $T(r) = 0.93\ (r/\mathrm{arcmin})^{0.127}$ keV, which is used in the deprojection of the surface brightness profile.

dance, temperature, column density, and normalization allowed to vary was used to fit the NPS emission. Since the NPS is in our Galaxy, we chose to let the column density acting on the emission from this component be a free parameter, since only a fraction of the total column density in the direction of NGC 4472 is the result of absorbing material between us and the NPS. We estimate that about one-third of the Galactic neutral hydrogen in the direction of NGC 4472 lies between us and the NPS, given a distance to the NPS of ~ 100 pc (Bingham 1967) and a Galactic latitude of 70°. This estimate assumes the Galactic N_{H} distribution model of Lockman, Hobbs, & Shull (1986), in which half the mass of the hydrogen is in clouds having a Gaussian distribution with a scale height of 135 pc and half the mass is in an exponential component with a scale height of 500 pc.

The results are shown in Table 2, along with 90% confidence levels. The temperature of 1.4 keV found for the Virgo emission component is somewhat lower than that found from an analysis of the *ROSAT* All-Sky Survey (Böhringer et al. 1994) and *Ginga* data (Koyama et al. 1991), although the large number of free parameters in this model precludes a tight constraint on the temperature. Rather tight constraints could be placed on the temperature of the NPS emission component, however. An accurate abundance could not be found for this component given the large number of free parameters of the fit and the very low temperature. The derived column density of 1.44×10^{20} cm^{-2} acting on this component is slightly lower than the measured total Galactic value, although higher than the estimated value of one-third the Galactic value. This does not seem an unreasonable value given the uncertainty in the distance to the NPS and the vertical distribution of Galactic hydrogen on small scales. The count rate for the background annulus is identical to that found from the *ROSAT* all-sky survey. In addition, the surface brightness derived for the Virgo component is consistent with the *Ginga* result. Perhaps surprisingly, there does not appear to be a significant gradient in the Virgo or NPS emission with position over the field of view of the detector. Nearly identical fluxes and count rates were found for both components from the northern and southern halves of the annulus.

5. SPATIAL ANALYSES OF NGC 4472, UGC 7636, AND THE X-RAY HOLE

5.1. *Surface Brightness Profiles of NGC 4472*

5.1.1. *Profile Avoiding Bow Shock Region*

For the purposes of deriving the profile of the X-ray surface brightness, the hard band PSPC image was used. Since most of the X-ray background is composed of low-energy events, eliminating the soft energy channels reduces the background by a large amount while only moderately reducing the source counts, thus increasing the signal-to-noise ratio of the surface brightness profile. Events due to scattered solar X-rays, long-term background enhancements, and particle background were removed and the image was corrected for vignetting according to the Snowden (1995) routines. The counts in annular slices between position angles 150° and 270° were summed. A background annulus between 35′ and 45′ was normalized to and subtracted from each slice. A profile was also generated for the HRI using a background region of 8.′5–11.′5. The two profiles were joined at 4′. The best-fit spectrum in the region 0.′5–4′ gave energy fluxes for the HRI and PSPC that agreed to within 9%. In addition, the slopes of the radial profiles for the HRI and PSPC were equal in that region.

Assuming a thermal spectrum of 1.07 keV and an abundance of 110% of solar (the best-fit values from a circular slice from 0′ to 18′), the counts-to-energy ratio was calculated and the surface brightness profile was obtained. Figure 3 shows the X-ray surface brightness profile in the photon energy band (0.52–2.02 keV) with 1 σ errors. The profile can be traced out to a distance of about 260 kpc in the southwest quadrant. There are two plateaus in the

TABLE 2

X-RAY EMISSION IN BACKGROUND ANNULUS[a]

Parameter	Virgo Component	North Polar Star Component
Temperature (keV)	1.4 (> 1.1)	0.15 (0.10–0.21)
Abundance ($Z/Z_{\odot}$)	0.1 (fixed)	0.03 (unconstrained)
Column density (10^{20} cm^{-2})	1.64 (fixed)	1.44 (0.85–2.46)
I_{X}[b] (10^{-15} ergs s^{-1} cm^{-2} arcmin^{-2})	2.4 (1.8–2.7)	5.3 (4.9–6.6)

[a] The annulus contained 27,378 total counts. For this model, $\chi^2 = 122.2$ for 133 degrees of freedom.
[b] 0.2–2.48 keV.

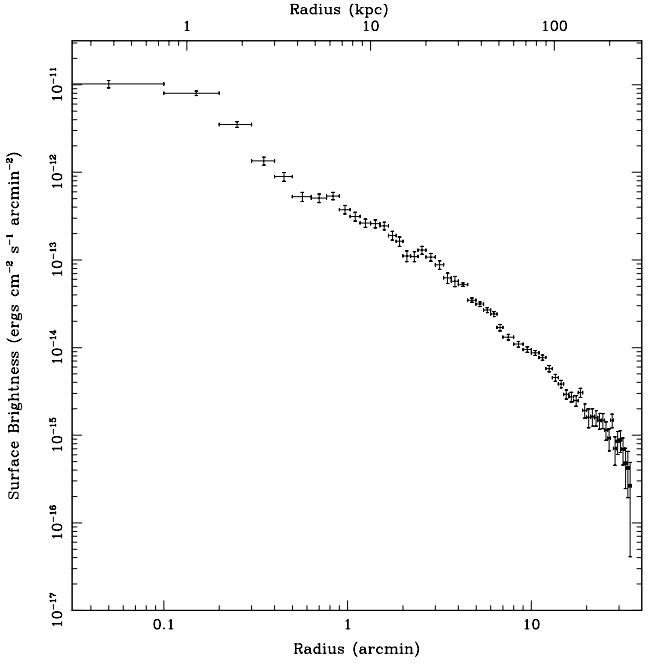

FIG. 3.—X-ray surface brightness profile in the 0.52–2.02 keV band from the merged HRI + PSPC data with 1 σ error bars.

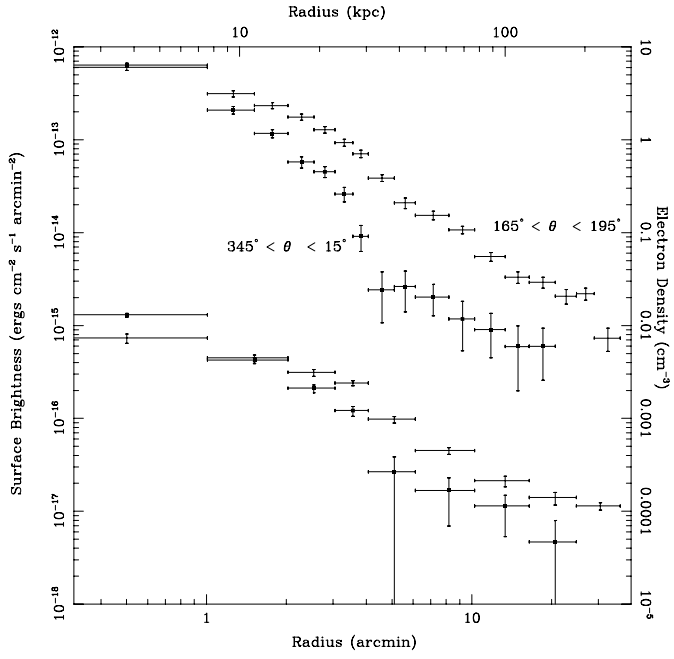

FIG. 4.—Surface brightness (*upper*) and electron density (*lower*) profiles from 30° slices north and south of the center of NGC 4472. The error bars on the electron density are the 10th and 90th percentile values from 1000 Monte Carlo simulations. Note the sharp drop-off in surface brightness and density at $\sim 3'$ in the northern slice.

X-ray emission at $r = 0.'7$ and $r = 1.'4$ due to filamentary structures at these radii in the X-ray image. There are also dips in the emission at $r = 2.'1$ and $r = 4.'8$. We attempted to fit a beta model to the surface brightness profile, but an adequate fit could not be obtained because of these features.

5.1.2. *Bow Shock Region Profile*

In § 3 we noted that there is a rapid decrease in the X-ray surface brightness with radius on the north side of NGC 4472. This decrease is shown in Figure 1. To quantify this rapid decline, we determined the X-ray surface brightness and electron density profiles for an angular wedge within $\pm 15°$ of north and south of the center of NGC 4472 from the PSPC hard band data (Fig. 4). The surface brightness and density are similar inside $\sim 3'$ in both slices. However, there is a sharp drop in the northern surface brightness at a radius of about $4'$, and the northern surface brightness profile flattens beyond this radius. From $\sim 6'$ outward the two profiles have similar slopes overall, with the southern slice contributing about 5 time more flux than the northern slice.

If the gas in the northern region is either being shocked, or compressed adiabatically, or mixed with hotter intracluster gas, the temperature in this region would be higher than in the undisturbed region. To test this possibility, we compared the temperature of the gas north of the galaxy (from position angles 270° to 90°) with the temperature of the gas in the unshocked southwest region. The same spectral model described in § 4.1 above was used to fit the spectra. For the inner $2.'5$, similar temperatures were found to the north and south. However, between $2.'5$ and $18'$, the temperature of the northern region of the galaxy was slightly higher ($1.41^{+0.29}_{-0.12}$ keV) than that in the southwest region ($1.13^{+0.05}_{-0.01}$ keV). The derived abundances were consistent between the two regions.

5.1.3. *Tail Region Profile*

In contrast to the rapid decline in X-ray surface brightness to the north of NGC 4472, this emission is more extended to the south. This extension is elongated to the southwest of the galaxy center, which is nearly perpendicular to the optical elongation of the galaxy (Fig. 1). The extension is illustrated in Figure 5, where the X-ray surface brightness was determined for 30° angular wedges southwest and southeast of the center of NGC 4472 from the PSPC hard band data. The profiles begin to diverge

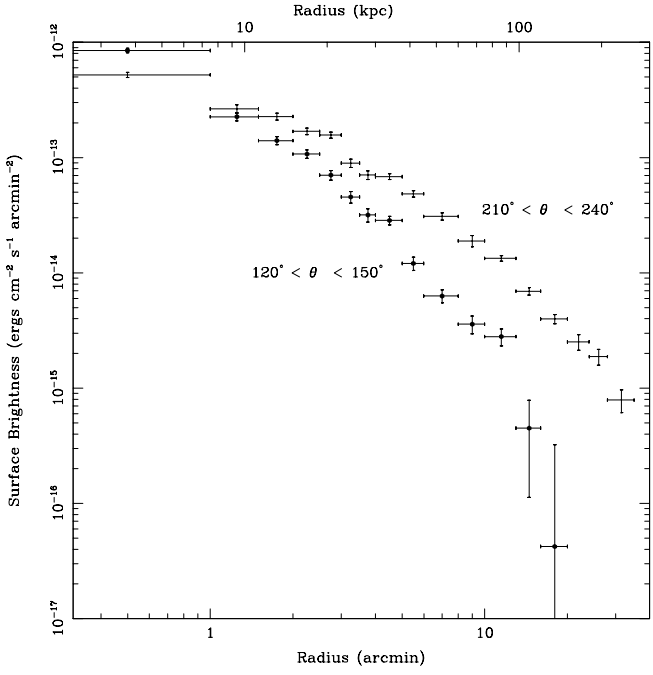

FIG. 5.—Surface brightness profiles from 30° slices southwest and southeast of the center of NGC 4472, with 1σ error bars. The extended emission in the southwest slice is evident.

around a few arcminutes, and by 15′ the southwest wedge is contributing over an order of magnitude more flux than the southeast wedge.

5.2. *Electron Density and Mass Profiles of NGC 4472*

If the X-ray emission is assumed to be spherically symmetric within the slice (150°–270°) region, we can deproject the surface brightness profile obtained in § 5.1.1 to yield the emissivity profile. The basic technique for doing this was developed by Fabian et al. (1981). The electron density profile can readily be derived from the emissivity profile if the temperature profile is known. The enhanced spectral resolution of the PSPC lends itself very well to this task. Using the power-law fit to the observed temperature profile in Figure 2, the resulting electron density profile is shown in Figure 6. The gas density profile can be integrated to give the mass of gas interior to any radius, $M_{\rm gas}(r)$, as shown in Figure 7. Note that we have determined the mass of the gas assuming that the 120° slice used in the analysis is representative of the entire galaxy, if it were not being distorted by interaction with Virgo cluster gas. Therefore, only the gas mass values within 4′ (where the contours are circularly symmetric) should be regarded as accurate. Because of the rapid decline in the X-ray surface brightness to the north, the mass values in Figure 7 at radii greater than 4′ may overestimate the actual total gas mass by 25%–30% and are designated by dotted lines to remind the reader of the uncertainty of the value.

If hydrostatic equilibrium is assumed and only gas pressure contributes to the support of the gas, the total gravitating mass in the system within radius r is given by

$$M(<r) = -\frac{rkT(r)}{\mu m_{\rm H} G}\left[\frac{d\ln\rho(r)}{d\ln r} + \frac{d\ln T(r)}{d\ln r}\right], \qquad (1)$$

where ρ is the gas density and μ is the mean molecular weight. Equation (1) was applied to the derived density and temperature profiles in NGC 4472. It was necessary to combine some of the bins in order to ensure a monotonically increasing gravitational mass profile. The accumulated gas and gravitational mass profiles are shown in Figure 7. Statistical errors on these quantities are not easily assigned since the errors in the emissivities at different radii are correlated by the deprojection. Therefore, a Monte Carlo technique (Arnaud 1988) has been adopted to assign errors to all quantities derived from the emissivity. The errors on the electron density, gas mass, and gravitational mass profiles represent the 10th and 90th percentile values from 1000 Monte Carlo simulations.

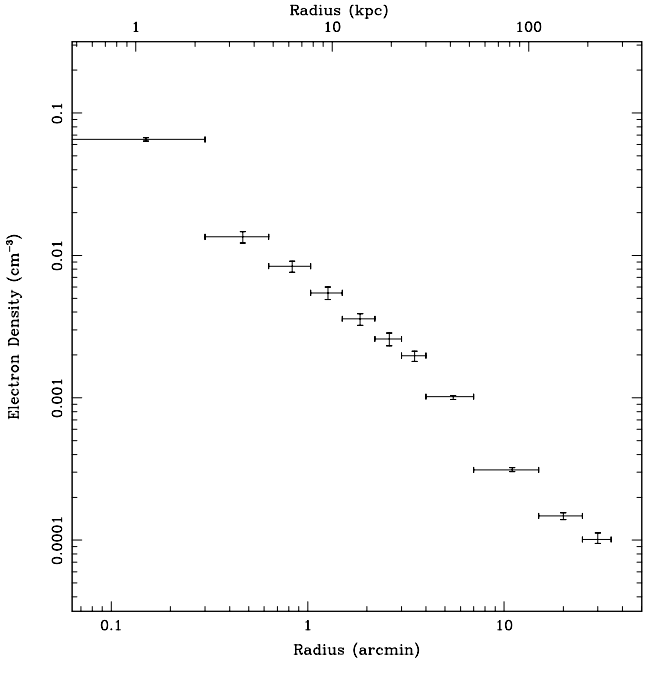

FIG. 6.—Deprojected electron density profile for NGC 4472. The error bars give the 10th and 90th percentile values from 1000 Monte Carlo simulations. Many of the bins in the surface brightness profile were combined in order to ensure a monotonically decreasing density profile.

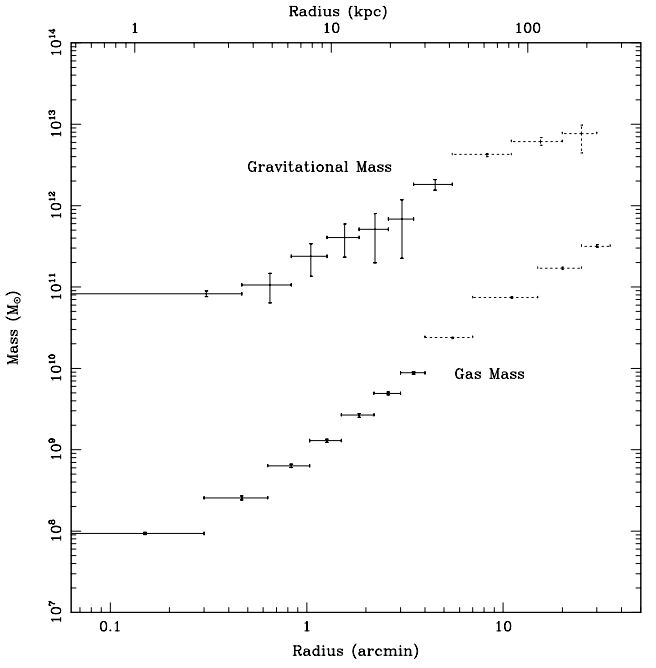

FIG. 7.—Profiles of the accumulated gas mass (*lower points*) and accumulated gravitational mass (*upper points*) in NGC 4472. The error bars are the 10th and 90th percentile values from 1000 Monte Carlo simulations. Dotted error bars represent mass values that are uncertain because of asymmetries in emission.

Mass values outside of 4′ might not be accurate, since the gas may not be in hydrostatic equilibrium at large radii. Once again, this is indicated by dotted lines in Figure 7. The total mass within 4.′5 is $(1.8 \pm 0.3) \times 10^{12}\ M_\odot$. Assuming an $R^{1/4}$ surface brightness distribution with an effective radius of 104″ and a total blue magnitude of 9.32 (Burstein et al. 1987), the blue luminosity within 4.′5 is $L_B = 1.46 \times 10^{11} L_{B,\odot}$. This yields a total mass-to-light ratio of 10–14 $M_\odot/L_{B,\odot}$ within 34 kpc, only about 2 times the canonical stellar mass-to-light ratio in elliptical galaxies. If we use the mass and blue luminosity values derived at 25′ (190 kpc), we get a mass-to-light ratio of 22–47 $M_\odot/L_{B,\odot}$, about 4–8 times the canonical stellar mass-to-light ratio. Again, we stress that the mass value at this large radius might not be accurate. However, the tentative conclusion that NGC 4472 possesses a dark halo is in agreement with previous X-ray and kinematical studies of NGC 4472 (Forman et al. 1985; Lowenstein 1992).

5.3. *Limit on the X-Ray Luminosity from UGC 7636*

The dwarf galaxy UGC 7636 is located 5.′5 southeast of NGC 4472 at R.A. = $12^{\rm h}30^{\rm m}01^{\rm s}$ and decl. = 7°55′50″ (J2000). This irregular galaxy shows evidence for recent star

formation and stripping of material due to either tidal or ram pressure interactions with NGC 4472 and its gaseous environment (e.g., Patterson & Thuan 1992). In addition, UGC 7636 is strongly deficient in H I gas as compared to other dwarf irregulars of similar optical luminosity.

We do not detect a significant deviation (either positive or negative) in the hard band PSPC surface brightness at the position of this galaxy. The lack of significant extra X-ray absorption at the position of UGC 7636 is consistent with the idea that UGC 7636 has been stripped of nearly all its gas. We derive upper limits on the 0.52–2.02 keV X-ray flux and luminosity of UGC 7636 of 1.8×10^{-15} ergs s^{-1} cm^{-2} and 1.4×10^{38} ergs s^{-1}, respectively. The upper limit on the decrease in flux is 9.6×10^{-15} ergs s^{-1} cm^{-2}, which corresponds to an upper limit on the excess absorbing column density toward the dwarf galaxy of 7.6×10^{20} cm^{-2}.

5.4. *X-Ray Hole Properties*

As mentioned in § 3, there is a region of reduced X-ray surface brightness (an X-ray hole) located 3.′1 southeast of the peak of emission in the nucleus of NGC 4472. Figure 8 gives a contour map of the HRI X-ray image of the center of NGC 4472 showing the hole. The center of this feature is located at R.A. = $12^h29^m55^s$ and decl. = 7°57′48″ (J2000). In the HRI, the hole has a size of 66″ × 44″ (8.3 kpc × 5.5 kpc) and is significant at the 3.6 σ level. The significance level was determined by comparing the count rate in the hole to the count rate in an annular slice 2.′6–3.′6 in extent and between position angles 90° and 180°. We have also examined the PSPC image for this feature. There is a 30% reduction in the surface brightness in a 1′ radius region at the corresponding position in the PSPC hard band image. The decrease is significant at the 5.1 σ level. When a highly smoothed PSPC hard band image is subtracted from the adaptively smoothed image (in order to bring out detail in the radially declining surface brightness profile), a hole in the X-ray surface brightness is readily apparent. A hole in the X-ray emission at this position was found in the soft band PSPC image, although poor statistics and asymmetric emission in this image make an accurate determination of the significance of the feature nearly impossible. We also examined the *Einstein* HRI archive image of NGC 4472 (Forman et al. 1984; Trinchieri et al. 1986), but found no evidence for absorption at this position. Table 3 gives the reduction ($\Delta I_X/I_X$) in the average surface brightness of X-rays at the position of this hole as derived from the HRI and the PSPC hard band, along with the 1 σ errors.

We performed a number of tests to determine if this X-ray reduction might be due to an instrumental effect in the HRI. We considered the data taken in 1992 and 1994 separately; each showed a reduction in surface brightness at this position, albeit with a reduced significance. We also divided the data into three segments of 10 ks each, and we found evidence for the hole in all three. While the reduction in surface brightness is not overwhelmingly significant in the HRI, the soft band PSPC, or the hard band PSPC individually, its presence in all three suggests that it may be a real feature. It is worth noting that there are six other significant depressions present in the HRI image (denoted by an "H" in Fig. 8), although only one is as significant as the depression described above. In addition, none of these other depressions are visible in the PSPC soft or hard band images.

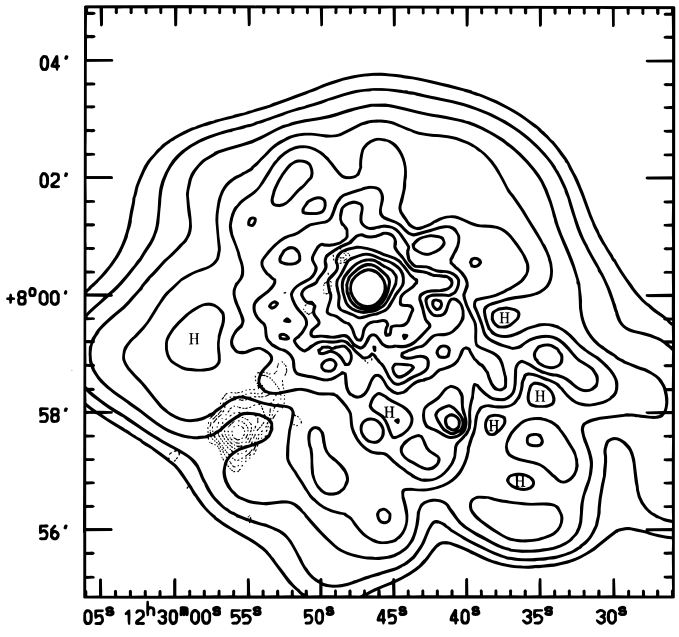

FIG. 8.—Adaptively smoothed, background-subtracted contour plot of the HRI image. A constant S/N of 5 per smoothing beam was used to determine the smoothing length. The hole in the X-ray emission described in the text is located at R.A. = $12^h29^m55^s$ and decl. = 7°57′48″ (J2000). Other holes in the X-ray emission are marked with an "H." The H I contours (*dotted lines*) from McNamara et al. (1994) are superposed on the X-ray contours.

We investigated the possibility that the reduction in the X-ray surface brightness is due to the physical displacement of the hot X-ray–emitting gas by a cloud of cooler gas. We assumed that the extent of this cloud along the line of sight is similar to its transverse extent in the plane of the sky. Assuming the hot gas density profile given by Figure 6, we found that even if the cloud displaced the densest gas along the line of sight, it would only reduce the surface brightness by ~10%, which is less than the observed reduction (see Table 3). The fact that the relative decrease in flux is larger

TABLE 3

X-RAY HOLE/H I CLOUD PROPERTIES

PARAMETER	X-RAY HOLE		H I CLOUD	
	HRI	PSPC Hard	Resolved[a]	Total[b]
$\Delta I_X/I_X$	0.82 (>0.58)	0.28 (0.23–0.34)	...	...
ΔN_H (10^{20} cm^{-2})	75 (>37)	13 (10–15)	4	N/A
Size	66″ × 44″	110″ × 110″	80″ × 40″	N/A
Mass (10^7 $M_\odot$)	300 (>150)	210 (170–250)	11	31

[a] VLA observations from McNamara et al. 1994.

[b] Greenbank 140 foot observations from Patterson & Thuan 1992.

in the HRI (which is also more soft X-ray sensitive than the PSPC) than in the hard band PSPC suggests that it is due to soft X-ray absorption, rather than reduced emission in this region. This would also argue against the possibility that the hole is a result of an irregularity in the Virgo background or an inhomogeneity in the flow of gas being removed from the galaxy (see § 6.2), since neither process should produce a significantly larger decrease in flux at soft energies than at hard energies. We determined the excess column density required to produce this X-ray hole by absorption, assuming that the absorbing material was in front of the X-ray emission from NGC 4472, and that the X-ray emission spectrum for NGC 4472 was that which best fit the emission from an annular slice of 2.'1–4.'1 in the southeast quadrant, using the thermal model described in § 4. The required excess columns and 1 σ confidence limits are given in Table 3. Obviously, if the absorbing gas were behind any portion of the X-ray emission, even larger columns would be required. Table 3 also gives the implied total mass of the absorbing material found by multiplying the average column by the area of the hole, assuming that it is located at the same distance as NGC 4472.

Note that the HRI and PSPC give rather different results for the required column density and size of the hole. This may be due at least partly to the small angular size of the X-ray hole, which is not resolved in the PSPC image. This might also suggest that a more extended H I component was detected with the PSPC. As another indication of consistency between the HRI and PSPC properties of the hole, we note that the HRI and PSPC give consistent masses for the absorbing material, owing to the fact that the hole appears larger in the PSPC than in the HRI. It is perhaps worth noting that although Table 3 gives the excess hydrogen columns implied by the X-ray hole, X-ray absorption at these energies is due primarily to heavy elements (e.g., oxygen). The hydrogen columns in Table 3 are derived assuming cosmic abundances. Also, the columns are nearly independent of the physical state of the absorbing material, as long as its temperature is $\lesssim 10^6$ K.

6. DISCUSSION

6.1. *The Bow Shock Region*

The center of the Virgo cluster (or the position of M87) lies almost directly to the north of NGC 4472. M87 is 4.°4 from NGC 4472 at a position angle of about 3°. This suggests that NGC 4472 (and perhaps some of the other galaxies in the southern region of the Virgo cluster) are presently falling in toward the center of the Virgo cluster to the north. The hot interstellar gas associated with NGC 4472 might be encountering resistance from Virgo cluster gas as it moves through this gas, and gas at the north side would be pushed back. If NGC 4472 were moving supersonically relative to the intracluster gas or the interstellar gas in NGC 4472, bow shock structures would be expected. If the motions were slower, the interstellar gas would be compressed adiabatically and pushed to the south. It is also possible that there might be a mixing layer containing both interstellar gas and more diffuse intracluster gas along the northern edge of the galaxy.

If the gas in the northern region had been compressed adiabatically, one would expect the density to increase as $\rho \propto T^{3/2}$, or by about 40% in this case (see § 5.1.2). Figure 4 shows that the X-ray surface brightness and density are always smaller to the north than the south at moderate to large radii. Recent models for ram pressure stripping from elliptical galaxies of Balsara, Livio, & O'Dea (1994) and Portnoy, Pistinner, & Shaviv (1993) predict this result. The Balsara et al. (1994) simulations show a double shock structure in front of the galaxy, which is not seen in NGC 4472. However, the scale of the inner shock structure is on the order of 10″ at the distance of the Virgo cluster. Although greater than the resolution of the HRI, annuli of this size yield too few X-ray counts to discern reliably any detail in the density profile at this level. Beyond this inner shock, the hydrodynamic models show a lower density on the bow of the galaxy compared to the tail. We also note that the intracluster density of Virgo is several times less than the density used by Balsara et al. (1994), which will have the effect of weakening the bow shock. Projection effects may also reduce the contrast in X-ray surface brightness in the shock region if the relative velocity is not in the plane of the sky. In any case, the fact that the gas in the bow region has a slightly higher temperature but a lower density than gas to the south shows that it has more entropy, and that it may have been heated either in a shock or by mixing with hotter Virgo intracluster gas.

If the rapid decrease in the gas density and the "bow shock" shape of the isophotes to the north of NGC 4472 are due to ram pressure from motion through the intracluster gas, then we would expect that the pressure at the interface between the galactic and intracluster gas would be approximately $P \approx \rho_{\rm ICM} v^2/2$, where $\rho_{\rm ICM}$ is the density of the intracluster gas and v is the relative velocity. The pressure at 4′ was estimated to be 1.6×10^{-12} dynes cm^{-2} from Figure 4 and the temperatures discussed above. The Virgo intracluster gas density was estimated to be 9×10^{-5} cm^{-3} from the *Ginga* surface brightness profile in the region around NGC 4472. Using these values for the intracluster gas density and the gas pressure in NGC 4472 at the interface, we estimate that the required relative velocity is

$$v \approx 1300 \left(\frac{P}{1.6 \times 10^{-12} \text{ dynes cm}^{-2}} \right)^{1/2} \times \left(\frac{\rho_{\rm ICM}}{1.9 \times 10^{-28} \text{ g cm}^{-3}} \right)^{-1/2} \text{km s}^{-1}, \quad (2)$$

which is a reasonable value for the infall velocity of NGC 4472 into the center of the Virgo cluster. Note that this velocity is derived solely from the observed pressure gradient induced by the ram pressure due to the motion of NGC 4472 through the intracluster medium.

By comparison, the observed radial velocity of NGC 4472 of 997 km s^{-1} is 295 km s^{-1} less than the radial velocity of M87 (Faber et al. 1989). The difference between the radial velocity of NGC 4472 and M87 might either indicate that NGC 4472 is well in front of the Virgo cluster (and the velocity difference is due to the Hubble flow) or that NGC 4472 is behind the center of the Virgo cluster and falling into the cluster. Recent distance determinations to NGC 4472 based on surface brightness fluctuations and planetary nebulae luminosities (Ciardullo, Jacoby, & Tonry 1993) suggest that NGC 4472 and M87 are at nearly the same distance. In this case, the difference in the radial velocity of NGC 4472 and M87 might be one component of the velocity of NGC 4472 relative to the ambient intracluster gas. This suggests that the remaining transverse velocity

component of NGC 4472 relative to M87 is about 1260 km s^{-1}, and the relative velocity of NGC 4472 makes an angle of approximately 13° relative to the plane of the sky. Given that the projected distance between NGC 4472 and M87 is ~ 2 Mpc, this small angle would require NGC 4472 to be only ~ 0.5 Mpc behind M87, a result not inconsistent with the surface brightness fluctuations and planetary nebulae luminosities distance determinations. Thus, NGC 4472 would appear to be moving nearly in the plane of the sky toward M87.

6.2. *The Tail Region*

The fact that the southwest extension discussed in § 5.1.3 is aligned perpendicular to the optical elongation of the galaxy argues that this southwest extension is not due to gas in hydrostatic equilibrium with an elliptical galactic potential well that is oriented in the same manner as the stellar distribution in the galaxy. In general, an extension of the gas to the south is naturally explained as a consequence of ram pressure. It is unlikely that very supersonic stripping due to this ram pressure is taking place, since this would require a velocity much greater than the sound speed within the intracluster medium (~ 1000 km s^{-1}). In addition, given that the mass-loss rate by stars in an elliptical galaxy is only on the order of 1 $M_\odot$ yr^{-1}, very supersonic stripping would remove all the gas from the galaxy on a timescale of $\sim 10^8$ yr. We would then have to be observing the galaxy at a very special point in its history, when stripping was just beginning. It is most likely that either slow, transonic stripping is occurring, or perhaps no stripping at all, with the pressure gradient induced by the intracluster gas pushing the galactic gas around in the gravitational potential without actually removing the gas from the galaxy. However, why should the extension be elongated to the southwest, rather than directly to the south (i.e., opposite to the apparent relative velocity)? This change in direction might be due to curvature in the orbital motion of NGC 4472, but there is no other bright galaxy in the area to produce this curvature.

It seems most likely that the orientation of the ram pressure tail of NGC 4472 to the southwest is due to the elliptical shape of the potential of the galaxy. The ram pressure acting on the north side of NGC 4472 will generate a pressure gradient within the interstellar gas in the galaxy. The interstellar gas will move in response to this gradient and to the gradient in the gravitational potential of the galaxy. If the pressure gradient makes an oblique angle relative to the principle axes of the elliptical galaxy, the flow of interstellar gas may be partially redirected along the path of least resistance out of the potential, which is the shortest axis of the elliptical galaxy. The degree to which this can occur depends on the relative sizes of the induced pressure gradient and the gradient in the gravitational potential. The overall change in the pressure induced by the ram pressure will be approximately $\Delta P \approx \rho_{\rm ICM} v^2/2$, where v is the velocity of NGC 4472 through the intracluster medium calculated in § 6.1. It is useful to compare this pressure difference to $\rho \Delta\phi$, where ρ is the density of the interstellar gas and $\Delta\phi$ is the gravitational potential difference across the galaxy. If $\Delta P \gg \rho \Delta\phi$, the ram pressure forces will overwhelm gravity, and the galactic gas would be removed in the direction of the relative velocity vector (to the south in this case) whatever the shape of the galaxy. If $\Delta P \ll \rho \Delta\phi$, ram pressure is ineffective and the interstellar gas would not be affected. However, if $\Delta P \approx \rho \Delta\phi$, then ram pressure forces and gravity are comparable in size, and the shape of the galactic potential may be important. In this case, the gas will tend to be pushed out of the center of the galaxy along the path of least resistance, which is the shortest axis of an elliptical galaxy. This would result in the ram pressure tail being oriented somewhere between the direction of the relative velocity and the direction of the minor axis of the galaxy in the same direction. From Figure 1, this situation would seem to apply to NGC 4472. We have compared ΔP and $\rho \Delta\phi$, using the gas density profile for the southwest region (Fig. 6) to derive ρ, our determination of the gravitating mass profile (Fig. 7) to determine $\Delta\phi$, and the value of the ram pressure implied by the distortion to the north of the galaxy (eq. [2]). We find that $\Delta P \ll \rho \Delta\phi$ for small radii, but that $\Delta P \approx \rho \Delta\phi$ from $\sim 10'$ outward. This is approximately the same radius at which the surface brightness profiles of the southwest and southeast regions begin to diverge significantly (Fig. 5).

Although these crude arguments are probably sufficient to show that the gas in NGC 4472 might be pushed out along the minor axis, detailed hydrodynamical simulations are needed to validate this hypothesis in more detail. Finally, it should be noted that it is possible that the southwest extension is not a result of interaction with Virgo gas, but an inhomogeneity in the Virgo gas itself at the position of NGC 4472.

6.3. *The* H I *Cloud and the X-Ray Hole*

The hole in the X-ray surface brightness discussed in § 5.4 is coincident with an H I cloud located midway between NGC 4472 and UGC 7636 (Sancisi et al. 1987). The contours of the H I cloud have been superposed on the X-ray contours in Figure 8. The measured velocity of the cloud of 470 ± 5 km s^{-1} (Patterson & Thuan 1992) lies between that of NGC 4472 (997 km s^{-1}; Faber et al. 1989) and UGC 7636 (276 ± 78 km s^{-1}; Huchra 1996). Thus, UGC 7636 is moving toward us relative to NGC 4472, and the cloud is at an intermediate velocity. McNamara et al. (1994) find that the H I cloud and UGC 7636 have very similar morphologies, and that UGC 7636 is devoid of any neutral hydrogen, which is most unusual for a dwarf irregular galaxy. The amount of H I detected in the cloud is consistent with that expected to be found in a noninteracting dwarf irregular, although at the lower end of the $M(\text{H I})/L_B$ range for field dwarf irregulars (Patterson & Thuan 1992). This naturally suggests that the H I cloud was removed from UGC 7636, either by tidal interaction with NGC 4472 or by ram pressure stripping caused by the motion of the dwarf through the hot gaseous halo around NGC 4472 (Sancisi et al. 1987). The simplest interpretation of the relative positions and velocities of NGC 4472, UGC 7636, and the H I cloud would be that UGC 7636 is on an orbit from behind (further away) and northwest of NGC 4472, has now passed around NGC 4472 to the southeast, and that the H I cloud was left behind (because of ram pressure stripping or possibly tidal stripping) at an intermediate position.

Given the positional agreement between the H I cloud and the X-ray hole and the evidence that the hole is due to absorption, it is natural to suggest that the absorbing material is associated with the cloud. Given that the hole is a significant reduction in the X-ray surface brightness (see Table 3), this would require that the H I cloud lie in front of NGC 4472. As noted above, this does not agree with the geometry that would explain the kinematics of NGC 4472,

UGC 7636, and the cloud in the most straightforward way, if the H I cloud was stopped close to the location where it was stripped. However, we show below that the cloud may have moved a considerable distance after being stripped. The observed radial velocity of the cloud differs significantly from that of NGC 4472, so it is unlikely that it has come to rest in the ambient hot gas.

In Table 3, the properties of the H I cloud are compared to the required properties of the X-ray absorber. McNamara et al. (1994) derived a mass of $1.1(\pm 0.1) \times 10^8$ $M_\odot$ for the cloud from VLA observations. Patterson & Thuan (1992) find a mass of $3.1(\pm 0.5) \times 10^8$ $M_\odot$ with the Greenbank 140 foot (42.7 m) telescope (both scaled to our adopted distance of 25.8 Mpc). The Greenbank single-dish measurement gives a better limit on the total 21 cm flux, but may include emission from a more spatially extended region. We find that the lower limit on the required mass of material to produce the absorption in the HRI exceeds the upper limit on the H I mass of the cloud by at least a factor of 5. Thus, if the X-ray hole is real and due to absorption by material in the H I cloud, this implies that most of the material in this cloud is not atomic hydrogen. The most likely alternative is that the bulk of the material in the cloud is molecular. Observations of the H I cloud with the IRAM 30 m radio telescope by Hutchmeier et al. (1994) failed to detect any CO (2–1) emission, but the authors state that their pointing was 45″ west of the center of the H I cloud. Given the small beam size of the IRAM 30 m telescope (13.″5; Downes 1989), these limits may not rule out a large amount of molecular gas in the H I cloud. CO observations centered on the H I cloud are clearly needed.

The X-ray observations of the gaseous atmosphere of NGC 4472 allow us to test the idea that the H I cloud was removed by ram pressure, and provide information on the subsequent deceleration of the cloud. The condition for ram pressure stripping of the gas from the irregular by the X-ray halo of NGC 4472 is given approximately by Gunn & Gott (1972) as

$$\rho_X V^2 \gtrsim 2\pi G \sigma_{\rm total}\, \sigma_{\rm gas}\ , \qquad (3)$$

where ρ_X is the X-ray gas mass density, V is the velocity of UGC 7636 relative to the ambient gas, and $\sigma_{\rm total}$ and $\sigma_{\rm gas}$ are the total and gas surface mass densities, respectively, of the irregular dwarf prior to the interaction. The radial component of the relative velocity is currently ≈ 700 km s^{-1}, so it seems reasonable to take $V \approx 1000$ km s^{-1}. We assume that the gas in UGC 7636 had the same column density as the X-ray–absorbing cloud, since the cloud is about the same size as the galaxy. This leads to $\sigma_{\rm gas} \approx 1.4 m_p (7.5 \times 10^{21}$ atoms cm$^{-2}) \approx 84\ M_\odot$ pc^{-2}. Patterson & Thuan (1992) find UGC 7636 to have a blue luminosity of $1.76 \times 10^8 L_{B,\odot}$. After scaling this value to our adopted distance of 25.8 Mpc and assuming an average dwarf irregular total mass–to–blue luminosity of 4.6 (Thuan 1985), we obtain a total preinteraction mass for UGC 7636 of $5.4 \times 10^9\ M_\odot$. This implies that $\sigma_{\rm gas} \approx 0.5 \sigma_{\rm total}$, which is in reasonable agreement with the observed gas fractions in dwarf irregular galaxies (Gallagher & Hunter 1989). The ram pressure condition is satisfied if the X-ray gas electron density is $\gtrsim 1.3 \times 10^{-2}$ cm^{-3}. Thus, ram pressure would be capable of stripping the gas from the irregular galaxy if the irregular galaxy passed within $\sim 0.'5$ of the center of NGC 4472 (see Fig. 6). A similar calculation using only the observed H I surface mass density shows that the gas could easily be stripped even at large distances from NGC 4472. It would appear that the presence of large amounts of molecular gas places rather tight constraints on the path of UGC 7636 through the X-ray halo of NGC 4472.

To what extent would one expect the stripped gas cloud to have been decelerated by ram pressure from the X-ray gas? Roughly speaking, the cloud would only be stopped after encountering a hot gas column at least equal to the cloud's column density. The column density of the hot gas through the center of NGC 4472 is about 4 times less than the column density of the cloud as measured with the HRI. Thus, it would appear that the intervening column of hot gas is too small to completely stop the stripped gas from UGC 7636, but might be expected to decelerate it somewhat. We note that the difference in the radial velocity between UGC 7636 and the H I cloud (≈ 200 km s^{-1}) is smaller than the difference between the cloud and NGC 4472 (≈ 500 km s^{-1}), which is consistent with these arguments. It should be noted, though, that this conclusion hinges on the assumption that a large amount of (presently) undiscovered molecular hydrogen is present in the cloud, and that the total column density of the cloud is given correctly by the X-ray observations. If the total column of the cloud were that seen in H I, the cloud should have been nearly completely decelerated in the X-ray gas. (The dynamical friction timescale is too long to be significant, even with our higher mass for the cloud.)

It is not clear whether the cloud will escape NGC 4472. The escape velocity from NGC 4472 at the projected radius of the cloud is about twice as great as the relative radial velocity between the cloud and NGC 4472, and it is likely that the cloud will undergo further deceleration because of ram pressure. If the cloud lies in front of the X-ray halo of NGC 4472 as the X-ray observations imply, the escape velocity might be lower. Without knowing the true radial distance of the cloud from NGC 4472 (and hence the efficacy of ram pressure to decelerate the cloud) nor the cloud's transverse velocity, it is difficult to predict whether the cloud can escape from NGC 4472 or will be accreted by the larger galaxy.

7. SUMMARY

We have analyzed a long *ROSAT* HRI image of the bright elliptical galaxy NGC 4472 in the southern Virgo cluster. We have also used the archival *ROSAT* PSPC observation to provide spectral information and additional spatial information.

NGC 4472 appears to be moving north through the Virgo intracluster gas and may be falling into the center of the Virgo cluster. There is a large asymmetry in the distribution of the X-ray emission, which was noted originally in the *Einstein* observations (Forman et al. 1985; Fabbiano 1989). To the north, the X-ray surface brightness falls off rapidly, and the X-ray contours have a "bow shock" shape. The temperature beyond 2.′5 in this bow shock region is somewhat higher than the temperature of the galaxy's southwest side, and the surface brightness and density are lower on the north side in agreement with previous numerical simulations of ram pressure stripping of elliptical galaxies in clusters. If this distortion is due to ram pressure from the Virgo cluster gas, the required intracluster gas density and galactic velocity of NGC 4472 are reasonable. Below this "bow shock" region, the X-ray emission of NGC 4472 are elongated in the southwest direction, which is perpendicular to

the major axis of the elliptical stellar distribution of the galaxy. We argue that ram pressure from the Virgo cluster gas is pushing the interstellar medium of NGC 4472 out along this path of least resistance in the galactic potential.

Spectral fits performed on annular slices (avoiding the bow shock region) yield a temperature profile with a drop at the center. This confirms the prediction of cooling flow models for this elliptical galaxy. As previously noted by Forman et al. (1993), the abundances were consistent with solar in all bins except the innermost bin, where cooling gas is probably a complicating factor.

We present surface brightness, electron density, gas mass, and gravitational mass profiles for NGC 4472 derived from the southwest region of the cluster, which we assume is not strongly affected by interaction with Virgo gas. The total gravitational mass at 34 kpc is $(1.8 \pm 0.3) \times 10^{12}\ M_{\odot}$, leading to a mass-to-light ratio of 10–14 $M_{\odot}/L_{B,\odot}$. If we use the mass value determined at 190 kpc, we infer that $M_{\rm dark}$ is 3–7 greater than $M_{\rm stars}$ if we adopt a stellar mass-to-light ratio of 6 $M_{\odot}/L_{B,\odot}$. But, the distorted shape of the X-ray emission from NGC 4472 makes the application of hydrostatic equilibrium at large radii very questionable.

NGC 4472 is embedded in Virgo intracluster gas and lies in the direction of the North Polar Spur. X-ray emission from both components is detected in a background annulus uncontaminated by emission from NGC 4472. A temperature of 0.15 keV was found for the NPS component, and a temperature of 1.4 keV was found for the Virgo gas component.

NGC 4472 is interacting with the dwarf irregular galaxy UGC 7636. There is no detectable evidence for an excess or deficit of X-ray flux at the position of the dwarf. It appears that an H I cloud located midway between the two galaxies was removed from the dwarf through tidal interaction or ram pressure stripping and is coincident with a hole in the X-ray emission from the X-ray halo of NGC 4472. The hole is present in the HRI and the PSPC hard band, although only marginally significant (2–5 σ) in each band. If the hole in the HRI and PSPC images is due to soft X-ray absorption, the total gaseous mass of the cloud must be at least $1.7 \times 10^{9}\ M_{\odot}$, far greater than its 21 cm H I mass. If the hole is a result of absorption from neutral and molecular hydrogen in the cloud, then the cloud must be located in front of the bulk of the X-ray emission from NGC 4472, and most of the absorbing material must be molecular hydrogen. A search for this molecular gas in CO would be very useful.

J. A. I. thanks David Frayer, Zhenping Huang, Richard Patterson, Eric Richards, Trinh Thuan, and an anonymous referee for useful comments and suggestions. We also thank Brian McNamara for kindly providing a FITS image of the VLA observation of the H I cloud. This research has made use of the Simbad database operated at CDS, Strasbourg, France. J. A. I. and C. L. S. were supported by NASA *ROSAT* grant NAG 5-1891. The optical image is from the National Geographic Society–Palomar Observatory Sky Survey (NGS-POSS), obtained using the Oschin Telescope at Palomar Mountain. The NGS-POSS was funded by a grant from the National Geographic Society to the California Institute of Technology. The plates were processed into the present compressed digital form with their permission. The Digitized Sky Survey was produced at the Space Telescope Science Institute under US Government grant NAG W-2166.

REFERENCES

Arnaud, K. A. 1988, in Cooling Flows in Clusters and Galaxies, ed. A. C. Fabian (Dordrecht: Kluwer), 31
Balsara, D., Livio, M., & O'Dea, C. P. 1994, ApJ, 437, 83
Bingham, R. G. 1967, MNRAS, 137, 157
Böhringer, H., Briel, U. G., Schwarz, R. A., Voges, W., Hartner, G., & Trümper, J. 1994, Nature, 368, 828
Burstein, D., Davies, R. L., Dressler, A., Faber, S. M., Stone, R. P. S., Lynden-Bell, D., Terlevich, R., & Wegner, G. 1987, ApJS, 64, 601
Ciardullo, R., Jacoby, G. H., & Tonry, J. L. 1993, ApJ, 419, 479
Downes, D. 1989, in Diffraction-Limited Imaging with Very Large Telescopes, ed. D. M. Alloin & J.-M. Mariotti (Dordrecht: Kluwer), 53
Fabbiano, G. 1989, ARA&A, 27, 87
Faber, S. M., Wegner, G., Burstein, D., Davies, R. L., Dressler, A., Lynden-Bell, D., & Terlevich, R. J. 1989, ApJS, 69, 763
Fabian, A. C., Hu, E. M., Cowie, L. L., & Grindlay, J. 1981, ApJ, 248, 47
Forman, W., Jones, C., David, L., Franx, M., Makishima, K., & Ohashi, T. 1993, ApJ, 418, L55
Forman, W., Jones, C., & Tucker, W. 1984, in Clusters and Groups of Galaxies, ed. F. Mardirossian, G. Giuricin, & M. Mezzetti (Dordrecht: Reidel), 297
———. 1985, ApJ, 293, 102
Forman, W., Schwarz, J., Jones, C., Liller, W., & Fabian, A. C. 1979, ApJ, 234, L27
Gallagher, J. S., III, & Hunter, D. A. 1989, AJ, 98, 806
Gunn, J. E., & Gott, J. R., III. 1972, ApJ, 176, 1
Hasinger, G., Turner, T. J., George, I. M., & Boese, G. 1992, GSFC OGIP Calibration Memo CAL/ROS/92-001, NASA
Huang, Z., & Sarazin, C. L. 1996, ApJ, 461, 622
Huchra, J. 1996, private communication
Hutchmeier, W. K., Bregman, J. N., Hogg, D. E., & Roberts, M. S. 1994, A&A, 281, 327
Kim, D.-W., & Fabbiano, G. 1995, ApJ, 441, 182
Kim, D.-W., Fabbiano, G., Mackie, G., & Norman, C. 1995, preprint
King, I. R. 1978, ApJ, 222, 1
Koyama, K., Takano, S., & Tawara, Y. 1991, Nature, 350, 135
Lauer, T. R. 1985, ApJ, 292, 104
Lockman, F. J., Hobbs, L. M., & Shull, J. M. 1986, ApJ, 301, 380
Lowenstein, M. 1992, ApJ, 384, 474
McNamara, B. R., Sancisi, R., Henning, P. A., & Junor, W. 1994, AJ, 108, 844
Morrison, R., & McCammon, D. 1983, ApJ, 270, 119
Patterson, R. J., & Thuan, T. X. 1992, ApJ, 400, L55
Plucinsky, P. P., Snowden, S. L., Briel, U. G., Hasinger, G., & Pfeffermann, E. 1993, ApJ, 418, 519
Portnoy, D., Pistinner, S., & Shaviv, G. 1993, ApJS, 86, 95
Rangarajan, F. V. N., Fabian, A. C., Forman, W. R., & Jones, C. 1995, MNRAS, 272, 665
Raymond, J. C., & Smith, B. W. 1977, ApJS, 35, 419
Sancisi, R., Thonnard, N., & Ekers, R. D. 1987, ApJ, 315, L39
Snowden, S. L. 1995, Cookbook For Analysis Procedures for *ROSAT* XRT/PSPC Observations of Extended Objects and the Diffuse Background
Stark, A. A., Gammie, C. F., Wilson, R. W., Bally, J., Linke, R. A., Heiles, C., & Hurwitz, M. 1992, ApJS, 79, 77
Thuan, T. X. 1985, ApJ, 299, 881
Trinchieri, G., Fabbiano, G., & Canizares, C. R. 1986, ApJ, 310, 637